Check for updates

ADVANCING EARTH AND SPACE SCIENCES

Geophysical Research Letters

RESEARCH LETTER
10.1029/2026GL124543

Reassessing Methanesulfonic Acid as a Sea Ice Proxy: An Example From the Weddell Sea Sector

R. M. Smith[1,2], Z. C. Weich[1,3], C. Giorio[2], C. S. Allen[1], and E. R. Thomas[1]

[1]British Antarctic Survey, Cambridge, UK, [2]Yusuf Hamied Department of Chemistry, University of Cambridge, Cambridge, UK, [3]School of Earth and Environmental Sciences, University of Cardiff, Cardiff, UK

Key Points:

- High-resolution record of methanesulfonic acid archived in the Gomez ice core from the Antarctic Peninsula
- Air mass back-trajectories and correlations with sea ice satellite observations indicate a Weddell Sea proxy source region
- Methanesulfonic acid signal reflects seasonal sea ice processes rather than annual maximum sea ice extent in the Weddell Sea

Supporting Information:

Supporting Information may be found in the online version of this article.

Correspondence to:

R. M. Smith and E. R. Thomas,
rosmit19@bas.ac.uk;
lith@bas.ac.uk

Citation:

Smith, R. M., Weich, Z. C., Giorio, C., Allen, C. S., & Thomas, E. R. (2026). Reassessing methanesulfonic acid as a sea ice proxy: An example from the Weddell Sea sector. *Geophysical Research Letters*, *53*, e2026GL124543. https://doi.org/10.1029/2026GL124543

Received 1 JUL 2026
Accepted 28 SEP 2026

Author Contributions:

Conceptualization: R. M. Smith, E. R. Thomas
Investigation: R. M. Smith, Z. C. Weich
Methodology: R. M. Smith, Z. C. Weich
Supervision: C. Giorio, C. S. Allen, E. R. Thomas
Writing – original draft: R. M. Smith, Z. C. Weich
Writing – review & editing: R. M. Smith, Z. C. Weich, C. Giorio, C. S. Allen, E. R. Thomas

© 2026 The Author(s). Geophysical Research Letters published by Wiley Periodicals LLC on behalf of American Geophysical Union.
This is an open access article under the terms of the Creative Commons Attribution License, which permits use, distribution and reproduction in any medium, provided the original work is properly cited.

Abstract Antarctic sea ice has declined since 2015, but placing this trend in a longer-term context remains challenging. Ice core methanesulfonic acid (MSA) offers a potential record of sea ice variability beyond the instrumental period, yet its applicability in sectors including the Weddell Sea remains unclear. We present an MSA record from the Gomez ice core on the southwest Antarctic Peninsula and combine air mass back-trajectories and satellite observations to reassess the MSA-sea ice relationship. Trajectory and spatial correlation analyses identify the central Weddell Sea as the dominant MSA source. We show that traditional correlations with northernmost sea ice extent are misleading in this region due to spatially complex seasonal ice dynamics; instead, the timing of autumn–winter ice advance and consolidation influences MSA formation during the following spring–summer. These findings highlight both the complexity of the MSA-sea ice relationship and its potential for reconstructing seasonal sea ice variability.

Plain Language Summary Antarctic sea ice has declined since 2015, but placing this change in a longer-term context remains challenging. Methanesulfonic acid (MSA), a chemical compound preserved in Antarctic ice cores, offers a record of past sea ice conditions, though early attempts to use it to track Weddell Sea ice had limited success. Here, we present a new MSA record from an Antarctic Peninsula ice core, combined with satellite sea ice observations and air mass movement modeling. We show that most of the MSA reaching this core originates from the central Weddell Sea, and that the common method comparing MSA to the northernmost sea ice extent does not work well in this region. Instead, the timing of autumn–winter sea ice growth influences MSA levels in the following spring and summer. These findings show that MSA can capture seasonal sea ice changes and help place recent Antarctic declines in a longer-term context.

1. Introduction

Since 2015, Antarctic sea ice has declined rapidly, prompting suggestions that the Southern Hemisphere sea ice system has crossed into a new low-extent state (Purich & Doddridge, 2023). This carries broad climate and ecological consequences. Sea ice controls the ocean-atmosphere exchange of moisture, heat, and momentum (Elvidge et al., 2021), drives bottom water formation (Marzocchi & Jansen, 2017), and modulates primary production throughout the Southern Ocean (SO) (Arrigo & Thomas, 2004).

The recent trends have unfolded against the backdrop of Antarctica's strong seasonal sea ice cycle. Sea ice extent (SIE) increases for ∼7 months through austral autumn–winter to a September maximum, then retreats for ∼5 months through austral spring–summer to a February minimum (Roach et al., 2022). Negative SIE anomalies have occurred in different seasons and regions: the 2022 record low affected the Ross and Weddell Sea (WS) sectors in February (Turner et al., 2022), while in 2023 the largest anomalies occurred in June–August across the Ross Sea, Bellingshausen Sea (BS), and WS (Josey et al., 2024).

Routine observations of Antarctic sea ice are limited to the satellite era, making it difficult to place recent trends in a longer-term climate context. Additionally, model simulations have struggled to reproduce the observations (Holmes et al., 2024). Ice core proxies for sea ice variability have been developed in an attempt to extend the sea ice record beyond the satellite era (Abram et al., 2013). Chief among these is methanesulfonic acid (MSA), a by-product of the atmospheric oxidation of dimethylsulfide (DMS), itself derived from dimethylsulfoniopropionate (DMSP) which performs antioxidant and osmo-protectant functions in marine phytoplankton (Lyon et al., 2016; Sunda et al., 2002; Trevena & Jones, 2012). MSA has an atmospheric lifetime of days-weeks, enabling atmospheric transport from the SO marine source to coastal and continental Antarctica (Preunkert et al., 2008). Early studies of MSA in continental snow and ice showed positive correlations with nearby winter

SIE in East (Curran et al., 2003; Foster et al., 2006; Welch et al., 1993; Xiao et al., 2015), and West Antarctica (Abram et al., 2010; Thomas & Abram, 2016). This has been attributed to the regulating role of sea ice upon primary productivity: melting sea ice in spring stratifies the surface ocean and releases iron, triggering widespread ice-edge phytoplankton blooms (Behera et al., 2020; Pellichero et al., 2017). Years with increased winter SIE may therefore see a larger area of stratified, iron-enriched surface ocean available to support DMS-producing blooms upon retreat. In this time-lagged relationship, winter sea ice preconditions the system for a high or low MSA season in the following spring-summer (Thomas et al., 2019).

The positive relationship between MSA and winter SIE does not hold at all ice core sites. Several cores near the Ross (Rhodes et al., 2009; Sinclair et al., 2014), Amundsen (Criscitiello et al., 2013) and Weddell (Abram et al., 2011) Seas contain MSA archives that reflect nearby polynya variability, open water area and local DMS sources. Elsewhere, non-sea ice factors (e.g., wind direction) override any MSA-sea ice signal altogether (Abram et al., 2007; Hezel et al., 2011). Interannual variability in DMS oxidants (OH, NO_3, BrO) represents an additional limitation that cannot be constrained from ice core records alone (Read et al., 2008). Careful site-specific investigation is necessary to determine the climate information contained in each MSA record.

Despite its promise as a sea ice proxy, MSA-based reconstructions have limited spatial coverage, with few records capturing changes in the WS (Thomas et al., 2019). Previous attempts to utilize Weddell-proximal MSA records proved challenging, as offshore winds can transport MSA away from many coastal ice core sites (Abram et al., 2007). However, early efforts to interpret the MSA-sea ice signal were hindered due to limited satellite data resolution (Thomas et al., 2019).

In this study, daily satellite data (1979–2004) and MSA archived in the Gomez ice core from the Antarctic Peninsula (AP) are used to re-evaluate MSA as a sea ice proxy. Despite its proximity to the BS coast, Gomez receives air masses and precipitation from both the BS and WS (Thomas & Bracegirdle, 2009). We assess mechanisms linking the Gomez record to WS sea ice, highlighting the potential for distal ice core records to capture seasonal sea ice variability.

2. Data and Methods

2.1. Ice Core Site and Drilling

The Gomez core was extracted to a depth of 136 m in January 2007, from a high-accumulation site in the southwest AP (73°59.40′S, 70°36.69′W), 1,400 m above sea level (Thomas et al., 2008) (Figure S1 in Supporting Information S1).

2.2. Analysis and Dating

Analysis was performed in 2007 using discrete samples (ion chromatography) at the British Antarctic Survey, and Continuous Flow Analysis at the Desert Research Institute (McConnell et al., 2002). The core sampling, analysis and dating is described in Text S1 and Table S1 in Supporting Information S1.

The MSA data were converted to annual average concentration, with each winter–winter average capturing peak summer MSA. The high resolution of the Gomez record allows filtering of low-level background values, isolating the seasonal MSA peaks and generating the sub-annual MSA_{summer} timeseries (see method in Text S1, Figures S1 and S2 in Supporting Information S1). The record presented relates to the upper 42 m of the core, spanning 1979–1980 to 2003–2004 and providing 25 years of satellite era overlap.

2.3. Meteorological Data

To examine atmospheric pathways at the Gomez site, air mass back-trajectories were generated using the HYbrid Single-Particle Lagrangian Integrated Trajectory model (Rolph et al., 2017; Stein et al., 2015) and ERA5 atmospheric reanalysis (Hersbach et al., 2020). One hundred twenty hour back-trajectories were generated every 48 hr between 1 January 1980 and 30 December 2004 from 100 m above ground level at the core site.

ERA5 monthly mean sea level pressure (MSLP) and 10 m zonal and meridional wind components for 1979–2004 were collated into 3-monthly means for correlation (Pearson's r) with the MSA_{summer} timeseries. All timeseries were linearly detrended first, with significance assessed using an effective sample size adjusted for lag-1 autocorrelation.

19448007, 2026, 20, Downloaded from https://agupubs.onlinelibrary.wiley.com/doi/10.1029/2026GL124543 by NICE, National Institute for Health and Care Excellence, Wiley Online Library on [23/10/2026]. See the Terms and Conditions (https://onlinelibrary.wiley.com/terms-and-conditions) on Wiley Online Library for rules of use; OA articles are governed by the applicable Creative Commons License

2.4. Satellite Data

The Gomez MSA record was compared to satellite observations of SIE and concentration (SIC). SIE is a binary metric (>15% = ice-covered); SIC reports the ice concentration (15%–100%) inside each pixel. Daily data spanning 1979–2004 were obtained from the NSIDC Sea Ice Index v3.0 (Fetterer et al., 2017), with a gridded spatial resolution of 25 × 25 km. Three approaches were tested for assembling the sea ice data. In each case, both the sea ice and MSA_{summer} timeseries were detrended prior to correlation using Pearson's *r*, with significance assessed using an effective sample size adjusted for lag-1 autocorrelation in both timeseries.

2.4.1. SIE_{north}

The first approach utilized SIE data. For each longitudinal column in each gridded map, the northernmost latitude of the SIE (SIE_{north}) was calculated (see Text S2 in Supporting Information S1). Ice conditions southward of this latitude were disregarded. Following previous MSA studies (Abram et al., 2007, 2010; Curran et al., 2003), daily SIE_{north} maps were aggregated into 10° longitudinal sectors (e.g., 110°W–100°W) and running 3-monthly means (e.g., January–March, February–April), to reduce high-frequency variability and capture a broader regional and seasonal signal of SIE. Each 10° sector's 3-monthly timeseries was correlated with MSA_{summer}.

2.4.2. SIC

A second method utilized SIC data and follows Thomas and Abram (2016). Three-monthly mean SIC maps were stacked and each pixel timeseries was correlated with MSA_{summer}. Unlike the SIE_{north} approach, this method captures sea ice presence and concentration variability at high spatial resolution throughout the sea ice zone, from consolidated pack (70%–100%) to loose pack (15%–30%). Ice-free years within each pixel's timeseries are represented by zeros that can influence the magnitude and apparent significance of Pearson's *r*; pixels affected by one or more zeros are therefore flagged in the results.

2.4.3. SIE Advance and Retreat Timing

A third method used daily SIE data to derive the timing of autumn–winter ice advance ($SIE_{advance}$) and spring–summer retreat ($SIE_{retreat}$). Following Stammerjohn et al. (2008), the day on which each grid cell exceeded (fell below) 15% SIC for 5 consecutive days was recorded as the day of advance (retreat), with the advance period defined as mid-February to mid-September and retreat as mid-September to mid-February of the following year. The resulting annual timing maps were stacked and each pixel timeseries was correlated with MSA_{summer}.

2.4.4. Time-Lagged Correlations

The MSA_{summer} timeseries was correlated with sea ice observations averaged over various time intervals. For clarity, the MSA peak is tied to December (T0), when DMS concentrations in SO surface waters are highest (Hulswar et al., 2022). Other months are referenced relative to December, for example, sea ice in the prior May–July is termed T − 7 to T − 5. Seasons are austral throughout.

3. Results

3.1. MSA Measurements

The Gomez MSA record exhibits strong seasonality. In the post-1979 section (upper 42 m) of the core, the average MSA concentration is 5.0 (±5.5 SD) ppb, comparable to similar elevation coastal sites (Segato et al., 2024). For the sub-annual MSA_{summer} timeseries, the mean satellite era concentrations increase to 10.1 (±3.7 SD) ppb (Table S1 in Supporting Information S1).

3.2. Back-Trajectories and Wind Correlations

The back trajectory analysis confirms that air masses arriving each year at Gomez originate from both sides of the AP, with slightly more than half (55.7%) from the BS. However, the air mass origins show clear seasonality (Figures 1i and 1j): easterly originating trajectories, sourced from the WS, account for 63.7% of arrivals in January but only 35.3% in September, with correspondingly higher trajectory density over the WS in summer (December–February) and in the BS in winter (June–August). This is consistent with the field correlations between

19448007, 2026, 20, Downloaded from https://agupubs.onlinelibrary.wiley.com/doi/10.1029/2026GL124543 by NICE, National Institute for Health and Care Excellence, Wiley Online Library on [23/10/2026]. See the Terms and Conditions (https://onlinelibrary.wiley.com/terms-and-conditions) on Wiley Online Library for rules of use; OA articles are governed by the applicable Creative Commons License

10.1029/2026GL124543

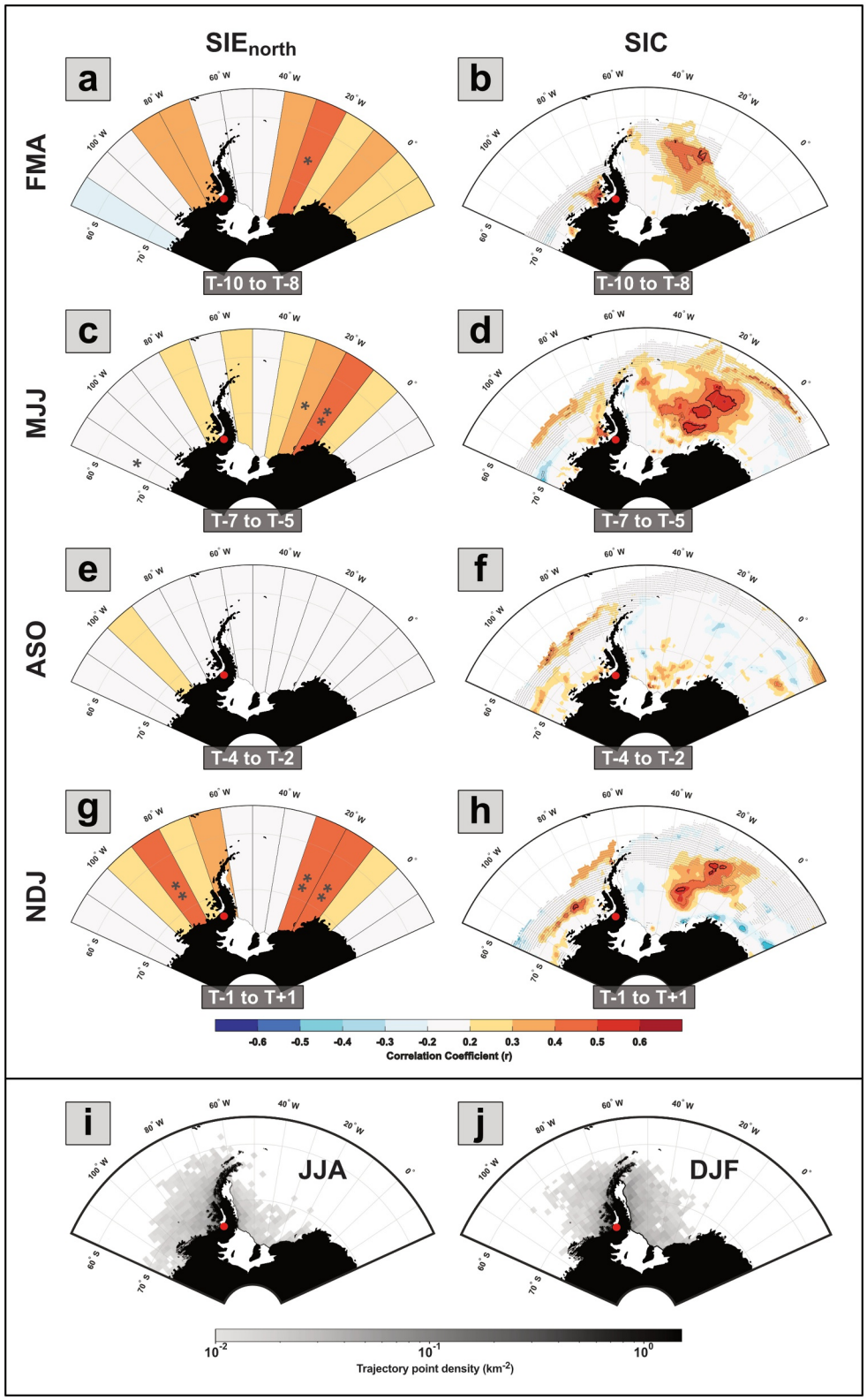

Figure 1. Correlation between MSA_{summer} and seasonal sea ice, alongside air mass back trajectory maps. Maps (a, c, e, and g) show correlations between MSA_{summer} and $SIE_{north,}$ where double (single) gray asterisks show significance at $p < 0.05$ ($p < 0.1$). Maps (b, d, f, and h) show correlation between MSA_{summer} and SIC, where thick black (thin black) contours show significance at $p < 0.05$ ($p < 0.1$). Gray stippling denotes grid cells where ≥1 year is represented by a zero (indicating no sea ice). Red dot shows Gomez core position. Maps (i, j) are back trajectory density plots, showing points per km^2. Three-letter codes at left indicate monthly windows.

19448007, 2026, 20, Downloaded from https://agupubs.onlinelibrary.wiley.com/doi/10.1029/2026GL124543 by NICE, National Institute for Health and Care Excellence, Wiley Online Library on [23/10/2026]. See the Terms and Conditions (https://onlinelibrary.wiley.com/terms-and-conditions) on Wiley Online Library for rules of use; OA articles are governed by the applicable Creative Commons License

MSA_{summer} and ERA5 meridional winds, which show enhanced southward flow along the southeastern flank of the AP during November–January associated with enhanced MSA_{summer} ($r = -0.5$, $p < 0.01$; Figure S3c in Supporting Information S1). The correlation between MSA_{summer} and MSLP shows no significant relationship during the spring–summer MSA transport window (Figure S3d in Supporting Information S1), confirming that no single, basin-scale synoptic pressure configuration dominates Gomez MSA_{summer} variability.

For the prior autumn window (March–May, T − 9 to T − 7), a coherent synoptic pattern associated with elevated MSA_{summer} comprises anomalously high MSLP over the central WS and strengthened offshore winds over Dronning Maud Land ($r = 0.4$–0.6, $p < 0.01$; Figures S3a and S3b in Supporting Information S1).

3.3. Relationship Between MSA_{summer} and SIE_{north}

There are positive correlations between MSA_{summer} and northernmost SIE (SIE_{north}), reaching $r = 0.4$–0.5 ($p < 0.05$) in the WS and BS (Figure 1). These correlations appear during the autumn ice advance period (T − 7 to T − 5) in the WS between 20°W and 10°W (Figure 1c), disappear through winter, and reappear in the spring–summer retreat season (T − 1 to T + 1) in both the WS (30°W and 10°W) and BS (90°W and 80°W) (Figure 1g). Sectors immediately east of the AP show no significant correlation, consistent with that region being dominated by multi-year ice.

3.4. Relationship Between MSA_{summer} and SIC

The spatial correlations between MSA_{summer} and three-monthly averaged SIC also show a positive relationship predominantly in the central WS, and to a much lesser degree in the BS (Figure 1). Correlations are strongest ($r = 0.5$–0.6, $p < 0.05$) in the central WS during May–July (T − 7 to T − 5). A timeseries exploring this relationship is shown in Figure S4 in Supporting Information S1. These correlations disappear through winter and reappear to a lesser extent in spring–summer (T − 1 to T + 1).

A minor region of significance is also shown for the earliest autumn window (T − 10 to T − 8, Figure 1b), but this region largely coincides with zero-year stippling, indicating that the prevalence of ice-free years at the ice margin means any correlation there should be interpreted with caution. However, the intervening temporal windows (Figure S5 in Supporting Information S1) reveal a progressive expansion of the significant positive correlation region throughout the ice advance phase toward May–July, accompanied by fewer years with "zero" sea ice.

3.5. Relationship Between MSA_{summer} and $SIE_{advance}$

The timing, speed, and spatial configuration of the advancing sea ice edge varies between years (Figures 2a and 2b), with particularly high interannual variability during the autumn months March–July (T − 9 to T − 5), as previously shown by Stammerjohn et al. (2008). Significant negative correlations between $SIE_{advance}$ and MSA_{summer} ($r = -0.4$ to -0.6, $p < 0.05$) are found in the central WS and, to a lesser degree, in the eastern BS (Figure 2c). Significant positive correlations are seen for the subsequent retreat season ($r = 0.4$ to 0.6, $p < 0.05$) in the same region (Figure 2d). Together, these indicate that years with an earlier advance and later retreat (i.e., a longer sea ice season) are associated with elevated MSA at Gomez.

4. Discussion

This study explores the complexity of the MSA-sea ice proxy relationship. Across three satellite sea ice metrics, significant correlations with MSA_{summer} are focused on the central WS and extend into the eastern BS. These correlations emerge first in the prior autumn and reappear in spring, suggesting that autumn sea ice conditions initiate a preconditioning signal that is carried through to the subsequent ice melt and marine productivity season. To our knowledge, ice core MSA has not previously been associated with sea ice in the prior autumn period. The following sections consider mechanisms underlying this relationship.

4.1. Wind-Driven Preconditioning and Transport

Wind dynamics exert a key control upon sea ice variability in the WS and wider SO (Blanchard-Wrigglesworth et al., 2021). The significant positive correlation between MSA_{summer} and MSLP during the prior March–May period (Figure S3b in Supporting Information S1) reinforces the role of winds and synoptic pressure in

19448007, 2026, 20, Downloaded from https://agupubs.onlinelibrary.wiley.com/doi/10.1029/2026GL124543 by NICE, National Institute for Health and Care Excellence, Wiley Online Library on [23/10/2026]. See the Terms and Conditions (https://onlinelibrary.wiley.com/terms-and-conditions) on Wiley Online Library for rules of use; OA articles are governed by the applicable Creative Commons License

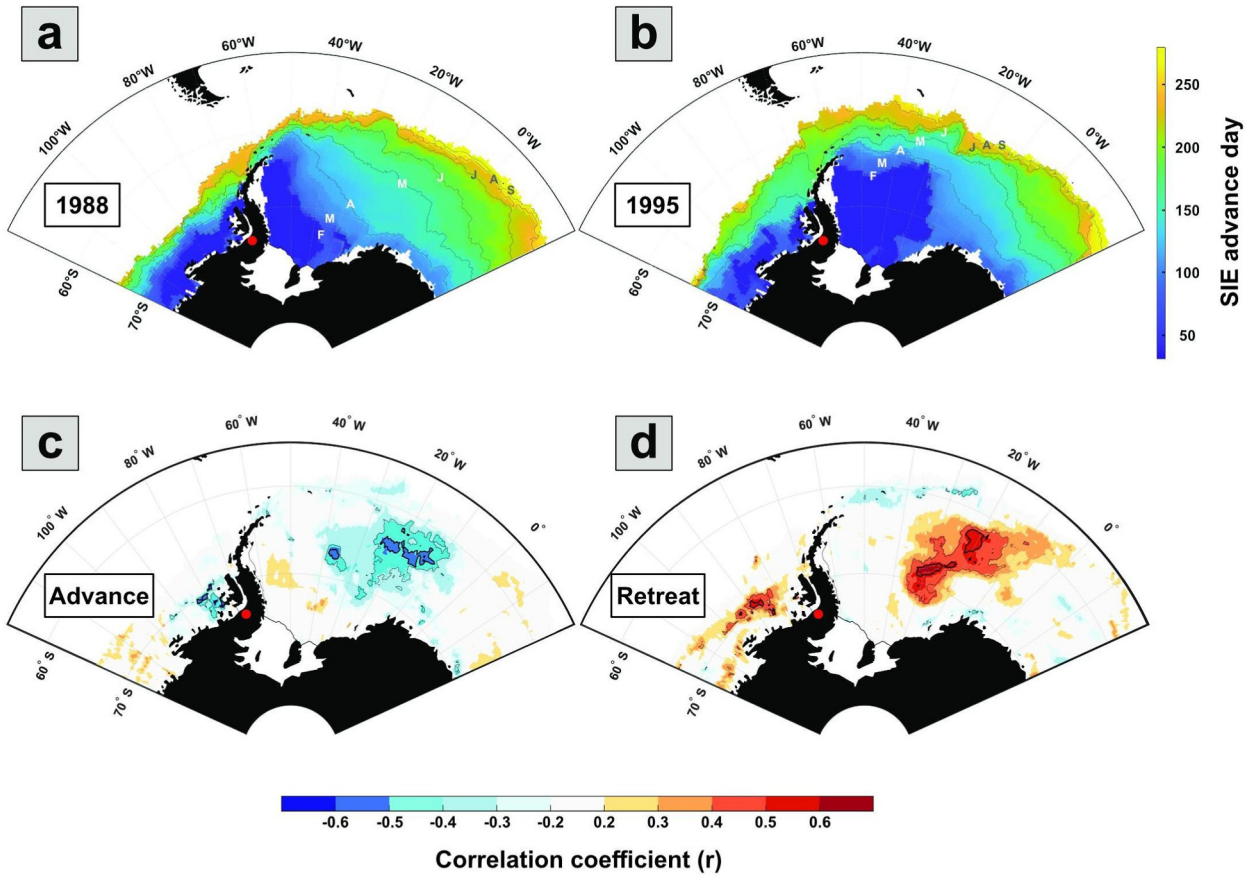

Figure 2. Maps describing sea ice edge advance and retreat timing and its relation to MSA_{summer}. Maps (a, b) show sea ice extent advance for 1988 and 1995, 2 years with contrasting patterns of sea ice growth. Colors show date of advance, letters denote end of each month. Maps (c, d) show correlation between MSA_{summer} and $SIE_{advance}$ and $SIE_{retreat,}$ respectively. In contrast to Figure 1, thick black (thin black) contours here delimit pixels where $p < 0.01$ ($p < 0.05$).

shaping the preconditioning pattern observed in the sea ice correlations. Increased seasonal MSLP (i.e., reduced storminess) allows sea ice to grow and consolidate more rapidly; the reverse (i.e., more frequent or intense low-pressure systems) favors the wind-driven export and wave-induced break-up of newly formed ice (Jena et al., 2022). Concurrently, the positive correlation with strengthened offshore winds over Dronning Maud Land (Figure S3a in Supporting Information S1) is consistent with enhanced coastal polynya activity and rapid new autumn sea ice production (Nghiem et al., 2016).

In spring–summer, the origin and frequency of airmasses reaching Gomez determines the regional significance and coherence of the MSA-sea ice signal. Back trajectory analysis reveals more frequent northeasterly atmospheric incursions (originating from the WS) during this transport window, due to a weakened Peninsula barrier effect (Orr et al., 2008) combined with eastward migration of the Amundsen Sea Low (Hosking et al., 2013) (Figure 1j, Text S3 in Supporting Information S1). The field correlations lend independent support to this seasonal transport pathway: MSA_{summer} is associated with enhanced southward flow along the eastern flank of the AP during the spring–summer period (Figure S3c in Supporting Information S1), consistent with the maritime, predominantly WS-sourced airmasses identified by the back trajectory analysis. Although these local winds are an additional inherent contributor to MSA_{summer} variability, the absence of any correlation with broader-scale MSLP during this transport window (Figure S3d in Supporting Information S1) indicates the signal is not governed by synoptic-scale transport; rather, synoptic pressure and regional winds in the prior autumn–winter remain the dominant driver of the original sea ice preconditioning.

19448007, 2026, 20, Downloaded from https://agupubs.onlinelibrary.wiley.com/doi/10.1029/2026GL124543 by NICE, National Institute for Health and Care Excellence, Wiley Online Library on [23/10/2026]. See the Terms and Conditions (https://onlinelibrary.wiley.com/terms-and-conditions) on Wiley Online Library for rules of use; OA articles are governed by the applicable Creative Commons License

4.2. Exploring the Gomez MSA Signal

4.2.1. Correlation Approaches

Although all three sea ice metrics show significant correlations focused primarily on the central WS region, they differ in their spatial sensitivity and the strength of correlations they resolve, reflecting fundamental differences in what each metric captures.

The strongest significant ($p < 0.05$) positive correlations occur during the prior autumn–winter advance period, May–July, and are most clearly resolved by the SIC metric (Figure 1d). In this temporal window, correlation coefficients within the interior WS pack exceed 0.5 across a broad, spatially coherent region, suggesting that Gomez MSA_{summer} may be related to the strength of prior seasonal ice advance and pack consolidation in this area. We note, however, that these correlations are moderate rather than strong; additional factors (e.g., atmospheric oxidant availability, wind strength and direction) are likely contributors to MSA variability at Gomez. The positive relationship disappears during the period of maximum winter SIE (Figures 1e and 1f), suggesting that the extent of winter ice is less important than the dynamics of the advancing autumn pack. It reappears during the spring retreat, but in a smaller significant region (Figure 1h).

The SIE_{north} metric offers a complementary perspective. Because it uses binary presence/absence data to derive the northernmost latitude of the sea ice "edge," it is free from the influence of zeros introduced by occasional absent sea ice at the ice margin in the SIC grid (see Section 2.4.2), making it better placed to interrogate the relationship between overall ice extent and MSA variability. This is particularly useful in the early advance (February–April) and late retreat (December–February) seasons, where ice-free years are most prevalent. However, this comes at the cost of spatial richness: because SIE_{north} captures only the northernmost latitudinal limit of the pack, it is insensitive to conditions within the interior, where the SIC signal is strongest. Consequently, SIE_{north} underestimates the association with autumn–winter (May–July) sea ice, because it samples from the northern margin where the correlation is weaker. In the WS this is a particular limitation, as sea ice advance does not proceed as a simple equatorward expansion parallel to latitudinal lines. The cyclonic gyre circulation produces spatially complex ice configurations, often generating a protruding arm of more consolidated ice in the north while looser pack persists to the south (Figure S6 in Supporting Information S1). Additionally, ice production in leads and openings within the interior pack is more important as a mode of seasonal ice increase in the WS relative to other sectors (Eisen & Kottmeier, 2000; Kimura & Wakatsuchi, 2011). The more spatially rich SIC metric, capturing both ice presence and degree of consolidation continuously across the full pack, is therefore better suited to resolving the full spatial complexity of sea ice variability in this basin.

For the WS, SIE data may be better applied using the $SIE_{advance}$ approach (Figure 2), which converts binary SIE values into a measure of the timing of sea ice cover expansion, while retaining high temporal (and spatial) resolution. This reveals that, alongside autumn–winter sea ice concentration, the point in the year at which the ice appears may also influence Gomez MSA. Figure 3 illustrates this using the six highest and lowest MSA_{summer} years in the 25-year record (years selected shown in Figure S7 in Supporting Information S1). Six-month mean autumn–winter ($T-9$ to $T-4$) SIC and $SIE_{advance}$ anomalies (relative to the 1979–2003 average) show that high MSA years are associated with earlier sea ice advance (~30 days earlier), and higher autumn–winter SIC (~10% above average) in the central WS (Figures 3a and 3b), with a weaker opposing pattern in low MSA years (Figures 3c and 3d). We conclude that the sea ice-MSA relationship operates differently at Gomez: rather than winter maximum SIE, Gomez MSA variability reflects earlier sea ice conditions as ice advances and thickens across the WS.

4.2.2. Why Might Autumn–Winter Sea Ice Affect Gomez MSA?

The association between MSA deposited at Gomez during the productivity period and prior sea ice conditions in the WS suggests a time-lagged relationship that is, in one sense, not new. MSA shows lagged positive correlations with prior winter maximum SIE in other cores (e.g., Law Dome (Curran et al., 2003), Ferrigno (Thomas & Abram, 2016), and three AP cores (Abram et al., 2010)). For those sites, a more northerly winter SIE is thought to expand the ocean area experiencing melt-induced phytoplankton blooms in the following spring–summer, driving enhanced DMS emissions and preconditioning the system for a "high-MSA" year. Yet at Gomez, the pre-conditioning appears more complex.

19448007, 2026, 20, Downloaded from https://agupubs.onlinelibrary.wiley.com/doi/10.1029/2026GL124543 by NICE, National Institute for Health and Care Excellence, Wiley Online Library on [23/10/2026]. See the Terms and Conditions (https://onlinelibrary.wiley.com/terms-and-conditions) on Wiley Online Library for rules of use; OA articles are governed by the applicable Creative Commons License

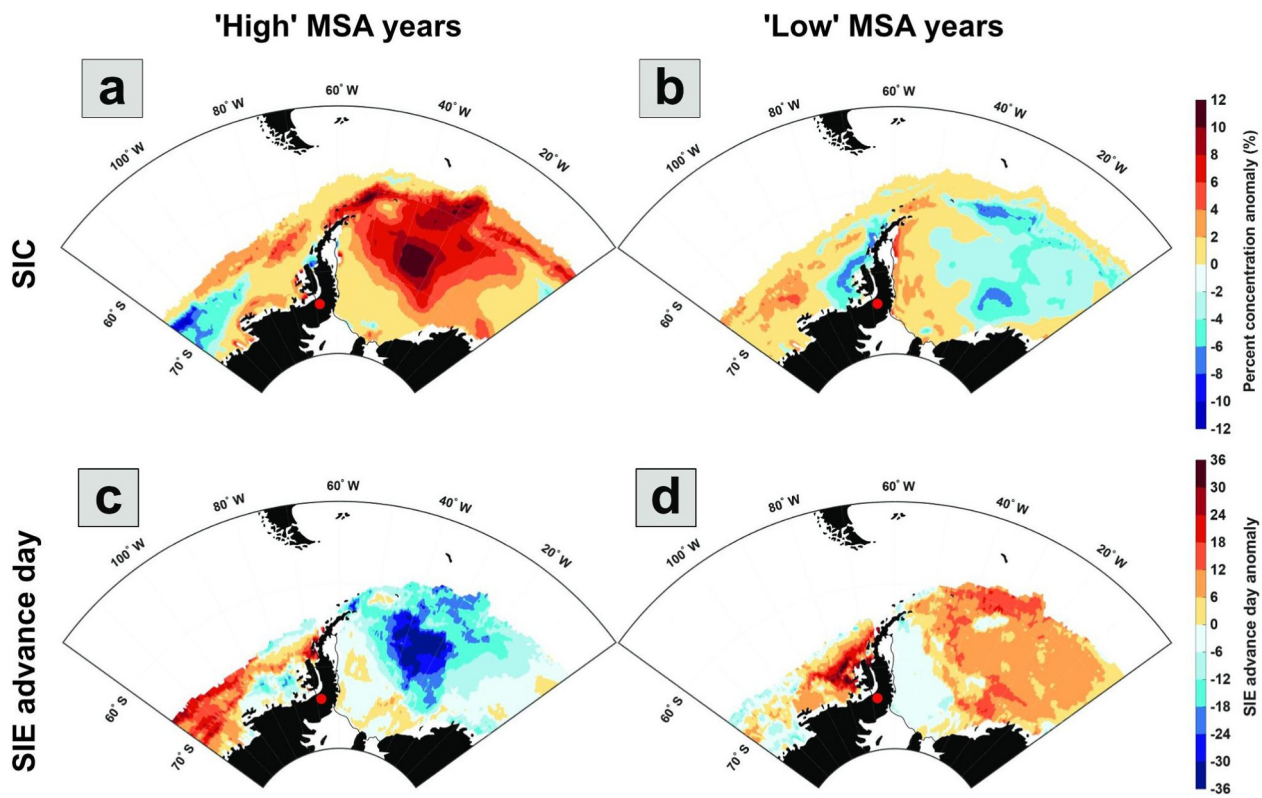

Figure 3. Maps showing SIC and $SIE_{advance}$ anomalies for highest and lowest MSA_{summer} years. (a, b) Show the average March–August (T − 9 to T − 4) SIC anomaly for the six highest and lowest MSA_{summer} years, relative to the average for this 6-monthly window throughout the 25-year period. (c, d) Show the same for the $SIE_{advance}$ metric.

Studies exploring the links between WS sea ice and summer phytoplankton productivity show that the relationship can be complex and spatially heterogeneous. Giddy et al. (2023) found significant positive correlations between annual sea ice concentration and summer bloom magnitude in the central WS (consistent with our results) but identified winter mixed-layer depth as a stronger predictor of bloom magnitude in many areas. This points to a key physical pathway: brine rejection during ice formation deepens the mixed layer, entraining iron-rich subsurface waters that fertilize subsequent spring blooms (Pellichero et al., 2017; Tagliabue et al., 2014). Early autumn ice growth may therefore amplify this mechanism, favoring deeper winter mixing and greater iron replenishment, whilst a longer ice growth period increases the seasonal ice volume available to drive springtime stratification upon melt.

These processes may also explain the reappearance of significant correlations during spring retreat (Figures 1h and 2d). Thicker, more consolidated ice that takes longer to melt may delay the start of the spring bloom, until higher solar irradiance can support a stronger initial pulse of phytoplankton activity (von Berg et al., 2020). A delayed retreat also pushes the spring bloom timing into the period of increased northeasterly wind transport toward Gomez (Section 4.1). Together, these physical processes provide a plausible preconditioning pathway linking autumn–winter sea ice to enhanced springtime DMS and MSA production within the Gomez atmospheric footprint.

An alternative mechanism involves the biogeochemical composition of the sea ice itself. During growth, sea ice scavenges and concentrates iron, organic matter, and phytoplankton biomass within developing brine channels (Asher et al., 2011; Lannuzel et al., 2015). The timing of sea ice growth may also matter; rapid ice formation earlier in autumn can enhance nutrient and particulate uptake because this material remains in suspension following the productive summer season (Janssens et al., 2016; Lannuzel et al., 2010). Rather than entering a dormant phase, wintertime biological activity drives progressive cycling and accumulation of nutrients and organic material as the ice consolidates and thickens (Audh et al., 2023; Tison et al., 2017). In spring, melting sea ice simultaneously releases its iron reservoir, fertilizing phytoplankton blooms (Geibert et al., 2010), and liberates

19448007, 2026, 20, Downloaded from https://agupubs.onlinelibrary.wiley.com/doi/10.1029/2026GL124543 by NICE, National Institute for Health and Care Excellence, Wiley Online Library on [23/10/2026]. See the Terms and Conditions (https://onlinelibrary.wiley.com/terms-and-conditions) on Wiley Online Library for rules of use; OA articles are governed by the applicable Creative Commons License

DMSP-rich algal biomass, with enzymatic cleavage of DMSP driving DMS release to the atmosphere (Trevena & Jones, 2006; Zemmelink et al., 2005). Earlier autumn formation and consolidation of sea ice may therefore capture nutrients and biomass before end-of-season depletion, effectively "locking in" a larger in-ice reservoir, whilst prolonging winter accumulation. This provides a complementary mechanism linking preconditioned autumn sea ice to spring–summer DMS release.

The MSA signal recorded at Gomez may reflect such distinct mechanisms for several reasons, relating both to the character of WS sea ice and to the core's geographical position. Relative to other SO sectors, the WS exhibits the largest and most rapid autumn–winter sea ice expansion, dominated by local thermodynamic freezing rather than dynamic advection (Kimura & Wakatsuchi, 2011; Kimura et al., 2023), providing a direct pathway for the preconditioning mechanisms described above. The Weddell Gyre circulation also retains and recirculates sea ice, such that ice forming in the central WS (where our correlations are strongest) likely remains in the basin until melt (Vernet et al., 2019). As suggested for iron in WS sea ice (Geibert et al., 2010), this circulation redistributes preconditioned ice across the basin, widening its influence. During retreat, melt within the interior pack plays a greater role in overall WS ice loss, compared to other sectors (Kimura et al., 2023), placing the DMS source closer to Gomez and strengthening the MSA–sea ice signal recorded at the core site.

5. Conclusions

This study presents a new assessment of the MSA sea ice proxy, using the high-resolution Gomez ice core record. Back trajectory analysis and satellite correlations identify the WS as the primary MSA source region. Testing three contrasting correlation approaches shows that linking MSA to the northernmost SIE produces misleading results in the WS, where cyclonic gyre circulation creates complex sea ice edge configurations. Spatial correlations with SIC and autumn–winter advance timing are more informative, and imply that earlier autumn–winter ice advance and consolidation in the central WS preconditions the system for high MSA in the subsequent spring–summer, unlike past studies that emphasize annual maximum SIE. This preconditioning scenario adds complexity to an already widely used sea ice proxy, whilst highlighting its potential for reconstructing seasonal sea ice variability in the WS.

Conflict of Interest

The authors declare no conflicts of interest relevant to this study.

Availability Statement

All data used in this study are available online. The Gomez ice core MSA record is available via the UK Polar Data Centre at https://doi.org/10.5285/64133f48-b358-418a-ad24-4718668cb2fe (Smith et al., 2026). ERA5 data (Hersbach et al., 2020) is available via the Copernicus Climate Change Service, Climate Data Store, as hourly (https://doi.org/10.24381/cds.adbb2d47, Hersbach et al., 2023a) and monthly (https://doi.org/10.24381/cds.f17050d7, Hersbach et al., 2023b) data sets. The NSIDC Sea Ice Index (G02135, Version 3) is available at https://doi.org/10.7265/N5K072F8 (Fetterer et al., 2017).

Acknowledgments
This work was funded by the UK Natural Environment Research Council (NERC). R. M. Smith was supported by NERC Grant NE/S007164/1. Z. Weich was supported by NERC GW4+ DTP - NE/S007504/1 (project ref. 2600312). The authors would like to thank the field team (P. Waite-Shores) for their help in the collection of the core and D. Tetzner for their constructive feedback on the manuscript. This manuscript was improved by the helpful comments of three reviewers.

References

Abram, N. J., Mulvaney, R., & Arrowsmith, C. (2011). Environmental signals in a highly resolved ice core from James Ross Island, Antarctica. *Journal of Geophysical Research*, *116*(D20), D20116. https://doi.org/10.1029/2011JD016147

Abram, N. J., Mulvaney, R., Wolff, E. W., & Mudelsee, M. (2007). Ice core records as sea ice proxies: An evaluation from the Weddell Sea region of Antarctica. *Journal of Geophysical Research*, *112*(D15), 15101. https://doi.org/10.1029/2006JD008139

Abram, N. J., Thomas, E. R., McConnell, J. R., Mulvaney, R., Bracegirdle, T. J., Sime, L. C., & Aristarain, A. J. (2010). Ice core evidence for a 20th century decline of sea ice in the Bellingshausen Sea, Antarctica. *Journal of Geophysical Research*, *115*(D23), D23101. https://doi.org/10.1029/2010JD014644

Abram, N. J., Wolff, E. W., & Curran, M. A. J. (2013). A review of sea ice proxy information from polar ice cores. *Quaternary Science Reviews*, *79*, 168–183. https://doi.org/10.1016/j.quascirev.2013.01.011

Arrigo, K. R., & Thomas, D. N. (2004). Large scale importance of sea ice biology in the Southern Ocean. *Antarctic Science*, *16*(4), 471–486. https://doi.org/10.1017/S0954102004002263

Asher, E. C., Dacey, J. W. H., Mills, M. M., Arrigo, K. R., Tortell, P. D., Dacey, J. W. H., et al. (2011). High concentrations and turnover rates of DMS, DMSP and DMSO in Antarctic sea ice. *Geophysical Research Letters*, *38*(23), L23609. https://doi.org/10.1029/2011GL049712

Audh, R. R., Fawcett, S. E., Johnson, S., Rampai, T., & Vichi, M. (2023). Rafting of growing Antarctic Sea ice enhances In-Ice biogeochemical activity in winter. *Journal of Geophysical Research: Oceans*, *128*(12), e2023JC019925. https://doi.org/10.1029/2023JC019925

19448007, 2026, 20, Downloaded from https://agupubs.onlinelibrary.wiley.com/doi/10.1029/2026GL124543 by NICE, National Institute for Health and Care Excellence, Wiley Online Library on [23/10/2026]. See the Terms and Conditions (https://onlinelibrary.wiley.com/terms-and-conditions) on Wiley Online Library for rules of use; OA articles are governed by the applicable Creative Commons License

Behera, N., Swain, D., & Sil, S. (2020). Effect of Antarctic sea ice on chlorophyll concentration in the Southern Ocean. *Deep Sea Research Part II: Topical Studies in Oceanography*, *178*, 104853. https://doi.org/10.1016/J.DSR2.2020.104853

Blanchard-Wrigglesworth, E., Roach, L. A., Donohoe, A., & Ding, Q. (2021). Impact of winds and Southern Ocean SSTs on Antarctic Sea ice trends and variability. *Journal of Climate*, *34*(3), 949–965. https://doi.org/10.1175/JCLI-D-20-0386.1

Criscitiello, A. S., Das, S. B., Evans, M. J., Frey, K. E., Conway, H., Joughin, I., et al. (2013). Ice sheet record of recent sea-ice behavior and polynya variability in the Amundsen Sea, west Antarctica. *Journal of Geophysical Research: Oceans*, *118*(1), 118–130. https://doi.org/10.1029/2012JC008077

Curran, M. A. J., Van Ommen, T. D., Morgan, V. I., Phillips, K. L., & Palmer, A. S. (2003). Ice core evidence for Antarctic Sea ice decline since the 1950s. *Science*, *302*(5648), 1203–1206. https://doi.org/10.1126/SCIENCE.1087888

Eisen, O., & Kottmeier, C. (2000). On the importance of leads in sea ice to the energy balance and ice formation in the Weddell Sea. *Journal of Geophysical Research*, *105*(C6), 14045–14060. https://doi.org/10.1029/2000JC900050

Elvidge, A. D., Renfrew, I. A., Brooks, I. M., Srivastava, P., Yelland, M. J., & Prytherch, J. (2021). Surface heat and moisture exchange in the marginal ice zone: Observations and a new parameterization scheme for weather and climate models. *Journal of Geophysical Research: Atmospheres*, *126*(17), e2021JD034827. https://doi.org/10.1029/2021JD034827

Fetterer, F., Knowles, K., Meier, W. N., Savoie, M., & Windnagel, A. K. (2017). Sea ice index (G02135, version 3) [Dataset]. *National Snow and Ice Data Center*. https://doi.org/10.7265/N5K072F8

Foster, A. F. M., Curran, M. A. J., Smith, B. T., Van Ommen, T. D., & Morgan, V. I. (2006). Covariation of sea ice and methanesulphonic acid in Wilhelm II land, east Antarctica. *Annals of Glaciology*, *44*, 429–432. https://doi.org/10.3189/172756406781811394

Geibert, W., Assmy, P., Bakker, D. C. E., Hanfland, C., Hoppema, M., Pichevin, L. E., et al. (2010). High productivity in an ice melting hot spot at the eastern boundary of the Weddell Gyre. *Global Biogeochemical Cycles*, *24*(3), GB3007. https://doi.org/10.1029/2009GB003657

Giddy, I. S., Nicholson, S. A., Queste, B. Y., Thomalla, S., & Swart, S. (2023). Sea-ice impacts inter-annual variability of phytoplankton bloom characteristics and carbon export in the Weddell Sea. *Geophysical Research Letters*, *50*(16), e2023GL103695. https://doi.org/10.1029/2023GL103695

Hersbach, H., Bell, B., Berrisford, P., Biavati, G., Horányi, A., Muñoz Sabater, J., et al. (2023a). ERA5 hourly data on single levels from 1940 to present [Dataset]. *Copernicus Climate Change Service (C3S) Climate Data Store (CDS)*. https://doi.org/10.24381/cds.adbb2d47

Hersbach, H., Bell, B., Berrisford, P., Biavati, G., Horányi, A., Muñoz Sabater, J., et al. (2023b). ERA5 monthly averaged data on single levels from 1940 to present [Dataset]. *Copernicus Climate Change Service (C3S) Climate Data Store (CDS)*. https://doi.org/10.24381/cds.f17050d7

Hersbach, H., Bell, B., Berrisford, P., Hirahara, S., Horányi, A., Muñoz-Sabater, J., et al. (2020). The ERA5 global reanalysis. *Quarterly Journal of the Royal Meteorological Society*, *146*(730), 1999–2049. https://doi.org/10.1002/QJ.3803

Hezel, P. J., Alexander, B., Bitz, C. M., Steig, E. J., Holmes, C. D., Yang, X., & Sciare, J. (2011). Modeled methanesulfonic acid (MSA) deposition in Antarctica and its relationship to sea ice. *Journal of Geophysical Research*, *116*(D23), 23214. https://doi.org/10.1029/2011JD016383

Holmes, C. R., Bracegirdle, T. J., Holland, P. R., Stroeve, J., & Wilkinson, J. (2024). Brief communication: New perspectives on the skill of modelled sea ice trends in light of recent Antarctic sea ice loss. *The Cryosphere*, *18*(12), 5641–5652. https://doi.org/10.5194/tc-18-5641-2024

Hosking, J. S., Orr, A., Marshall, G. J., Turner, J., & Phillips, T. (2013). The influence of the Amundsen–Bellingshausen Seas low on the climate of west Antarctica and its representation in coupled climate model simulations. *Journal of Climate*, *26*(17), 6633–6648. https://doi.org/10.1175/JCLI-D-12-00813.1

Hulswar, S., Simó, R., Galí, M., Bell, T. G., Lana, A., Inamdar, S., et al. (2022). Third revision of the global surface seawater dimethyl sulfide climatology (DMS-Rev3). *Earth System Science Data*, *14*(7), 2963–2987. https://doi.org/10.5194/essd-14-2963-2022

Janssens, J., Meiners, K. M., Tison, J. L., Dieckmann, G., Delille, B., & Lannuzel, D. (2016). Incorporation of iron and organic matter into young Antarctic sea ice during its initial growth stages. *Elementa*, *4*, 000123. https://doi.org/10.12952/journal.elementa.000123

Jena, B., Bajish, C. C., Turner, J., Ravichandran, M., Anilkumar, N., & Kshitija, S. (2022). Record low sea ice extent in the Weddell Sea, Antarctica in April/May 2019 driven by intense and explosive polar cyclones. *npj Climate and Atmospheric Science*, *5*(1), 19. https://doi.org/10.1038/s41612-022-00243-9

Josey, S. A., Meijers, A. J. S., Blaker, A. T., Grist, J. P., Mecking, J., & Ayres, H. C. (2024). Record-low Antarctic sea ice in 2023 increased ocean heat loss and storms. *Nature*, *636*(8043), 635–639. https://doi.org/10.1038/s41586-024-08368-y

Kimura, N., Onomura, T., & Kikuchi, T. (2023). Processes governing seasonal and interannual change of the Antarctic sea-ice area. *Journal of Oceanography*, *79*(2), 109–121. https://doi.org/10.1007/s10872-022-00669-y

Kimura, N., & Wakatsuchi, M. (2011). Large-scale processes governing the seasonal variability of the Antarctic sea ice. *Tellus A: Dynamic Meteorology and Oceanography*, *63*(4), 828–840. https://doi.org/10.1111/j.1600-0870.2011.00526.x

Lannuzel, D., Grotti, M., Abelmoschi, M. L., & van der Merwe, P. (2015). Organic ligands control the concentrations of dissolved iron in Antarctic sea ice. *Marine Chemistry*, *174*, 120–130. https://doi.org/10.1016/J.MARCHEM.2015.05.005

Lannuzel, D., Schoemann, V., De Jong, J., Pasquer, B., Van Der Merwe, P., Masson, F., et al. (2010). Distribution of dissolved iron in Antarctic sea ice: Spatial, seasonal, and inter-annual variability. *Journal of Geophysical Research*, *115*(G3), 3022. https://doi.org/10.1029/2009JG001031

Lyon, B. R., Bennett-Mintz, J. M., Lee, P. A., Janech, M. G., & Ditullio, G. R. (2016). Role of dimethylsulfoniopropionate as an osmoprotectant following gradual salinity shifts in the sea-ice diatom Fragilariopsis cylindrus. *Environmental Chemistry*, *13*(2), 181–194. https://doi.org/10.1071/EN14269

Marzocchi, A., & Jansen, M. F. (2017). Connecting Antarctic sea ice to deep-ocean circulation in modern and glacial climate simulations. *Geophysical Research Letters*, *44*(12), 6286–6295. https://doi.org/10.1002/2017GL073936

McConnell, J. R., Lamorey, G. W., Lambert, S. W., & Taylor, K. C. (2002). Continuous ice-core chemical analyses using inductively coupled plasma mass spectrometry. *Environmental Science and Technology*, *36*(1), 7–11. https://doi.org/10.1021/es011088z

Nghiem, S. V., Rigor, I. G., Clemente-Colón, P., Neumann, G., & Li, P. P. (2016). Geophysical constraints on the Antarctic sea ice cover. *Remote Sensing of Environment*, *181*, 281–292. https://doi.org/10.1016/J.RSE.2016.04.005

Orr, A., Marshall, G. J., Hunt, J. C. R., Sommeria, J., Wang, C. G., van Lipzig, N. P. M., et al. (2008). Characteristics of summer airflow over the Antarctic Peninsula in response to recent strengthening of westerly circumpolar winds. *Journal of the Atmospheric Sciences*, *65*(4), 1396–1413. https://doi.org/10.1175/2007JAS2498.1

Pellichero, V., Sallée, J. B., Schmidtko, S., Roquet, F., & Charrassin, J. B. (2017). The ocean mixed layer under Southern Ocean sea-ice: Seasonal cycle and forcing. *Journal of Geophysical Research: Oceans*, *122*(2), 1608–1633. https://doi.org/10.1002/2016JC011970

Preunkert, S., Jourdain, B., Legrand, M., Udisti, R., Becagli, S., & Cerri, O. (2008). Seasonality of sulfur species (dimethyl sulfide, sulfate, and methanesulfonate) in Antarctica: Inland versus coastal regions. *Journal of Geophysical Research*, *113*(D15), D15302. https://doi.org/10.1029/2008JD009937

19448007, 2026, 20, Downloaded from https://agupubs.onlinelibrary.wiley.com/doi/10.1029/2026GL124543 by NICE, National Institute for Health and Care Excellence, Wiley Online Library on [23/10/2026]. See the Terms and Conditions (https://onlinelibrary.wiley.com/terms-and-conditions) on Wiley Online Library for rules of use; OA articles are governed by the applicable Creative Commons License

Purich, A., & Doddridge, E. W. (2023). Record low Antarctic sea ice coverage indicates a new sea ice state. *Communications Earth & Environment*, *4*(1), 1–9. https://doi.org/10.1038/s43247-023-00961-9

Read, K. A., Lewis, A. C., Bauguitte, S., Rankin, A. M., Salmon, R. A., Wolff, E. W., et al. (2008). DMS and MSA measurements in the Antarctic boundary layer: Impact of BrO on MSA production. *Atmospheric Chemistry and Physics*, *8*(11), 2985–2997. https://doi.org/10.5194/acp-8-2985-2008

Rhodes, R. H., Bertler, N. A. N., Baker, J. A., Sneed, S. B., Oerter, H., & Arrigo, K. R. (2009). Sea ice variability and primary productivity in the Ross Sea, Antarctica, from methylsulphonate snow record. *Geophysical Research Letters*, *36*(10), L10704. https://doi.org/10.1029/2009GL037311

Roach, L. A., Eisenman, I., Wagner, T. J. W., Blanchard-Wrigglesworth, E., & Bitz, C. M. (2022). Asymmetry in the seasonal cycle of Antarctic sea ice driven by insolation. *Nature Geoscience*, *15*(4), 277–281. https://doi.org/10.1038/s41561-022-00913-6

Rolph, G., Stein, A., & Stunder, B. (2017). Real-time environmental applications and display sYstem: READY. *Environmental Modelling & Software*, *95*, 210–228. https://doi.org/10.1016/J.ENVSOFT.2017.06.025

Segato, D., Thomas, E. R., Tetzner, D., Jackson, S., Moser, D. E., Turetta, C., et al. (2024). Investigating halogens and MSA in the Southern Hemisphere: A spatial analysis. *Atmospheric Environment*, *319*, 120279. https://doi.org/10.1016/J.ATMOSENV.2023.120279

Sinclair, K. E., Bertler, N. A. N., Bowen, M. M., & Arrigo, K. R. (2014). Twentieth century sea-ice trends in the Ross Sea from a high-resolution, coastal ice-core record. *Geophysical Research Letters*, *41*(10), 3510–3516. https://doi.org/10.1002/2014GL059821

Smith, R. M., Weich, Z. C., & Thomas, E. R. (2026). Annual and sub-annual average methanesulphonic acid (MSA) concentration for the upper 42m (spanning 1979-2004) of the Gomez ice core, Antarctic Peninsula (version 1.0) [Dataset]. *NERC EDS UK Polar Data Centre*. https://doi.org/10.5285/64133f48-b358-418a-ad24-4718668cb2fe

Stammerjohn, S. E., Martinson, D. G., Smith, R. C., Yuan, X., & Rind, D. (2008). Trends in Antarctic annual sea ice retreat and advance and their relation to El Niño–Southern Oscillation and southern annular mode variability. *Journal of Geophysical Research*, *113*(C3), 3–90. https://doi.org/10.1029/2007JC004269

Stein, A. F., Draxler, R. R., Rolph, G. D., Stunder, B. J. B., Cohen, M. D., & Ngan, F. (2015). NOAA's HYSPLIT atmospheric transport and dispersion modeling system. *Bulletin of the American Meteorological Society*, *96*(12), 2059–2077. https://doi.org/10.1175/BAMS-D-14-00110.1

Sunda, W., Kieber, D. J., Kiene, R. P., & Huntsman, S. (2002). An antioxidant function for DMSP and DMS in marine algae. *Nature*, *418*(6895), 317–320. https://doi.org/10.1038/nature00851

Tagliabue, A., Sallée, J. B., Bowie, A. R., Lévy, M., Swart, S., & Boyd, P. W. (2014). Surface-water iron supplies in the Southern Ocean sustained by deep winter mixing. *Nature Geoscience*, *7*(4), 314–320. https://doi.org/10.1038/ngeo2101

Thomas, E. R., & Abram, N. J. (2016). Ice core reconstruction of sea ice change in the Amundsen-Ross Seas since 1702 A.D. *Geophysical Research Letters*, *43*(10), 5309–5317. https://doi.org/10.1002/2016GL068130

Thomas, E. R., Allen, C. S., Etourneau, J., King, A. C. F., Severi, M., Winton, V. H. L., et al. (2019). Antarctic sea ice proxies from marine and ice core archives suitable for reconstructing sea ice over the past 2000 years. *Geosciences*, *9*(12), 506. https://doi.org/10.3390/geosciences9120506

Thomas, E. R., & Bracegirdle, T. J. (2009). Improving ice core interpretation using in situ and reanalysis data. *Journal of Geophysical Research*, *114*(D20), D20116. https://doi.org/10.1029/2009JD012263

Thomas, E. R., Marshall, G. J., & McConnell, J. R. (2008). A doubling in snow accumulation in the western Antarctic Peninsula since 1850. *Geophysical Research Letters*, *35*, L01706. https://doi.org/10.1029/2007GL032529

Tison, J. L., Schwegmann, S., Dieckmann, G., Rintala, J. M., Meyer, H., Moreau, S., et al. (2017). Biogeochemical impact of snow cover and cyclonic intrusions on the winter Weddell Sea ice pack. *Journal of Geophysical Research: Oceans*, *122*(12), 9548–9571. https://doi.org/10.1002/2017JC013288

Trevena, A. J., & Jones, G. B. (2006). Dimethylsulphide and dimethylsulphoniopropionate in Antarctic sea ice and their release during sea ice melting. *Marine Chemistry*, *98*(2–4), 210–222. https://doi.org/10.1016/J.MARCHEM.2005.09.005

Trevena, A. J., & Jones, G. B. (2012). DMS flux over the Antarctic sea ice zone. *Marine Chemistry*, *134–135*, 47–58. https://doi.org/10.1016/J.MARCHEM.2012.03.001

Turner, J., Holmes, C., Harrison, T. C., Phillips, T., Jena, B., Reeves-Francois, T., et al. (2022). Record low Antarctic sea ice cover in February 2022. *Geophysical Research Letters*, *49*(12), e2022GL098904. https://doi.org/10.1029/2022GL098904

Vernet, M., Geibert, W., Hoppema, M., Brown, P. J., Haas, C., Hellmer, H. H., et al. (2019). The Weddell Gyre, Southern Ocean: Present knowledge and future challenges. *Reviews of Geophysics*, *57*(3), 623–708. https://doi.org/10.1029/2018rg000604

von Berg, L., Prend, C. J., Campbell, E. C., Mazloff, M. R., Talley, L. D., & Gille, S. T. (2020). Weddell Sea phytoplankton blooms modulated by sea ice variability and polynya formation. *Geophysical Research Letters*, *47*(11), e2020GL087954. https://doi.org/10.1029/2020GL087954

Welch, K. A., Mayewski, P. A., & Whitlow, S. I. (1993). Methanesulfonic acid in coastal Antarctic snow related to sea-ice extent. *Geophysical Research Letters*, *20*(6), 443–446. https://doi.org/10.1029/93GL00499

Xiao, C., Dou, T., Sneed, S. B., Li, R., & Allison, I. (2015). An ice-core record of Antarctic sea-ice extent in the southern Indian Ocean for the past 300 years. *Annals of Glaciology*, *56*(69), 451–455. https://doi.org/10.3189/2015AOG69A719

Zemmelink, H. J., Houghton, L., Dacey, J. W. H., Worby, A. P., & Liss, P. S. (2005). Emission of dimethylsulfide from Weddell Sea leads. *Geophysical Research Letters*, *32*(23), 1–4. https://doi.org/10.1029/2005GL024242

19448007, 2026, 20, Downloaded from https://agupubs.onlinelibrary.wiley.com/doi/10.1029/2026GL124543 by NICE, National Institute for Health and Care Excellence, Wiley Online Library on [23/10/2026]. See the Terms and Conditions (https://onlinelibrary.wiley.com/terms-and-conditions) on Wiley Online Library for rules of use; OA articles are governed by the applicable Creative Commons License